Scale Dependence of Omniphobic Mesh Surfaces

Shreerang S. Chhatre, Wonjae Choi, Anish Tuteja, Kyoo-Chul (Kenneth) Park, Joseph M. Mabry, Gareth H. McKinley, Robert E. Cohen**

[*] Prof. R. E. Cohen, Shreerang S. Chhatre, Dr. Anish Tuteja, Department of Chemical Engineering, Massachusetts Institute of Technology, Cambridge, MA, 02139, USA

E-mail: recohen@mit.edu

[*] Prof. G. H. McKinley, Dr. Wonjae Choi, Kyoo-Chul (Kenneth) Park, Department of Mechanical Engineering, Massachusetts Institute of Technology, Cambridge, MA, 02139, USA

E-mail: gareth@mit.edu

Dr. Joseph M. Mabry, Space and Missile Propulsion Division, Air Force Research Laboratory, Edwards Air Force Base, CA 93524, USA

* To whom correspondence should be addressed:

REC: Room 66-554, 77 Massachusetts Ave, Cambridge, MA 02139, Tel.: +1-617-253-3777; Fax: +1-617-258-8224, E-mail: recohen@mit.edu

GHM: Room 3-250, 77 Massachusetts Ave, Cambridge, MA 02139, Tel.: +1-617-258-0754; Fax: +1-617-258-8559, E-mail: gareth@mit.edu

RECEIVED DATE (to be automatically inserted after your manuscript is accepted if required according to the journal that you are submitting your paper to)

ABSTRACT

We provide a simple design chart framework to predict the apparent contact angle on a textured surface in terms of the equilibrium contact angle on a chemically identical smooth surface and the details of the surface topography. For low surface tension liquids like methanol (γ_{lv} = 22.7 mN/m) or octane (γ_{lv} = 21.6 mN/m), a solid-liquid-air composite interface on textured surface is inherently metastable. Thus on application of a sufficient pressure difference (*e.g.* an externally applied pressure or a sufficiently large Laplace pressure at small droplet size) the metastable composite interface transitions to a fully-wetted interface. A dimensionless robustness factor is used to quantify the breakthrough pressure difference necessary to disrupt a metastable composite interface and to predict *a priori* the existence of a robust composite interface. The impact of length scale (radius of the cylindrical features R varying from 18 to 114 microns) and the feature spacing ratio ($D^* = (R+D)/R$ varying from 2.2 to 5.1, where $2D$ is the spacing between the cylindrical features) on the robustness is illustrated by performing contact angle measurements on a set of dip-coated wire-mesh surfaces, which provide systematically quantifiable cylindrical texture. The design chart for a given feature size R shows how the two independent design parameters, surface chemistry as revealed in the equilibrium contact angle and texture spacing embodied in the dimensionless spacing ratio (D^*), can be used to develop surfaces with desirably large values of apparent contact angle and robustness of the metastable composite interface. Most revealing is the scaling of the robustness with the dimensionless parameter ℓ_{cap} / R (where $\ell_{cap} = \sqrt{\gamma_{lv} / \rho g}$ is the capillary length) which indicates clearly why, in the consideration of self-similar surfaces, 'smaller is better' for producing omniphobic surfaces that resist wetting by liquids with low surface tension.

KEYWORDS: Superhydrophobicity, Oleophobicity, Robustness factor, Design chart.

Introduction

There has been recently a significant amount of research directed towards achieving superhydrophobic and oleophobic textured surfaces. The optimal design of such surfaces involves a combination of good material or coating selection in order to minimize the surface energy of the solid (γ_{sv}) and an optimal choice of surface texture, including recognition of the important role of re-entrant curvature [1-8] of the designed surface topography. There are a few reports in the literature that systematically discuss the impact of surface texture on wettability.[6-24] By optimizing the interaction between the textured surface and contacting liquids, surfaces with a wide range of wettability starting from super-wetting (apparent contact angle $\theta^* \approx 0°$) to super-non-wetting surfaces ($\theta^* > 150°$), can be produced. Low surface tensions liquids like methanol ($\gamma_{lv} = 22.7$ mN/m) or octane ($\gamma_{lv} = 21.6$ mN/m) wet most surfaces and for such liquids, the impact of the surface texture on wettability is critical. For a selected type of textured surface, the separate role of feature size and relative spacing, as well as the independent contribution of surface chemistry can be highlighted most effectively using a suitably-constructed framework for presenting measured values of apparent contact angle with various contacting liquids. The present work shows how these ideas can be incorporated into a graphical framework for the design of surface textures and coatings for enhancing the apparent contact angle (θ^*) and breakthrough pressure (P_b).[6-8, 25, 26] The analysis reveals the value of making the feature size of the surface texture as small as possible at any fixed combination of relative topographical spacing and surface chemistry.

The wettability of textured surfaces is quantified in terms of the apparent contact angle (θ^*) displayed on the surface. For a liquid droplet with a solid-liquid-air composite interface, the contact angle is computed by using the Cassie-Baxter[21] (CB) relation given as $\cos\theta^* = r_\phi \phi_s \cos\theta_E + \phi_s - 1$.[3, 7, 23] Here r_ϕ is the roughness of the wetted area, ϕ_s is the area fraction of the liquid-air interface occluded by the solid texture, and θ_E is the equilibrium contact angle of the selected liquid on a chemically identical smooth surface. Previous work [1, 6-8, 27] has shown clearly that it is possible to sustain a composite interface on a re-entrant surface texture (*i.e.* a surface with multivalued topography) even when $\theta_E < 90°$,[7] because the

force balance given by Young's equation[28] can be satisfied locally. In general, if the equilibrium contact angle of a liquid on the smooth solid surface is θ_E and the local texture angle is ψ (angle between a local tangent to the solid surface and the horizontal, measured through the solid texture), it is possible to support a composite interface when $\theta_E > \psi$.

Model re-entrant lithographic surfaces have been made previously by a variety of routes,[1, 6, 29] but they are expensive and difficult to mass produce. On the contrary, woven and non-woven textiles are commonly available and represent a class of inexpensive re-entrant textured surfaces for which ψ varies continuously from 180 to 0° around the perimeter of the cylindrical fiber. Numerous research groups have demonstrated that textiles prepared from, or coated with, low surface energy materials (γ_{sv}) can lead to superhydrophobic [23, 30, 31] and/or oleophobic [6, 7, 9, 25, 26, 32-34] surfaces. Commercial fabric structures are available in various types of weaves, fabric materials, fiber diameter and fiber bundle size and can be modeled geometrically using an idealized cylindrical texture.[10, 23, 25, 26] For a surface with a cylindrical texture characterized by radius R and inter-cylinder spacing $2D$, the CB relation can be rearranged into a more convenient form,[7, 23, 25, 26]

$$\cos\theta^* = -1 + \frac{1}{D^*}\left[(\pi - \theta_E)\cos\theta_E + \sin\theta_E\right] \qquad (1)$$

where $r_\phi = (\pi - \theta_E)/\sin\theta_E$, $\phi_s = R\sin\theta_E/(R+D)$, $D^* = (R+D)/R$.

For a texture that is composed of features that are not flat-topped posts, we note that the surface texture variables, r_ϕ and ϕ_s that appear in the CB relation are functions of the equilibrium contact angle (θ_E) and are therefore dependent on the properties of the contacting liquid and the surface coating. On the contrary, the dimensionless spacing ratio (D^*) in Equation (1) is a purely geometric parameter which quantifies the openness of the weave. The repellency of fabric surfaces to water droplets (with very high equilibrium contact angles θ_E) was modeled by Kawase et. al. by considering specific topographical details like the warp, weft, and the type of weave.[22] Here we have modeled the fabrics using the one dimensional model first considered by Cassie and Baxter[21] due to its simplicity and applicability over the whole range of equilibrium contact angles ($0° \le \theta_E \le 180°$).

Incorporation of the robustness criterion into the design framework

The CB relation (Equation (1)) can be used only when the existence of a solid-liquid-air composite interface is assured. Derivation of the CB relation assumes a flat air-liquid interface, whereas in reality this interface can sag significantly under the influence of a pressure differential across the curved liquid-air interface either due to the Laplace pressure or an externally applied pressure.[6, 7, 35] If this sagging becomes severe, the bulging air-liquid interface may touch the next level of underlying solid texture and transition to a fully wetted interface. The tendency to resist the sagging of the air-liquid interface or robustness against wetting can be quantified in terms of a dimensionless robustness factor (A^*).[7] This parameter compares the ratio of the breakthrough pressure (P_b) to a reference pressure ($P_{ref} = 2\gamma_{lv} / \ell_{cap}$), where ℓ_{cap} is the capillary length ($\ell_{cap} = \sqrt{\gamma_{lv} / \rho g}$), γ_{lv} is the liquid surface tension and ρg is the specific weight. The reference pressure (P_{ref}) is close to the minimum pressure differential across a millimetric scale liquid droplet. For an array of cylinders with radius R and inter-cylinder spacing $2D$, the robustness factor (A^*) can be calculated using the following expression.[7, 25, 26]

$$A^* = \frac{P_b}{P_{ref}} = \frac{\ell_{cap}}{R(D^* - 1)}\left[\frac{(1 - \cos\theta_E)}{(D^* - 1 + 2\sin\theta_E)}\right] \qquad (2)$$

The robustness factor is a function of the equilibrium contact angle on a chemically identical smooth surface (θ_E), the geometrical spacing ratio (D^*) introduced above, and the ratio of capillary length (ℓ_{cap}) to the feature length-scale (R) of the solid's surface texture. Values of $A^* \lesssim 1$ indicate that a drop sitting on the composite fibrous surface will spontaneously transition to a fully-wetted interface.

Experimental Section

Coating methodology – Fluorodecyl POSS[36] (polyhedral oligomeric silsesquioxane) molecules consist of silsesquioxane cages surrounded by eight 1H,1H,2H,2H-heptadecafluorodecyl groups. A smooth fluorodecyl POSS surface has one of the lowest solid surface energy values reported to date ($\gamma_{sv} \approx 10$

mN/m), due to the high density of perfluorinated carbon atoms present in the eight alkyl chains surrounding the silsesquioxane cages.[7] To generate thin, uniform and flexible coatings of fluorodecyl POSS on the textures to be studied, a commercially available Tecnoflon fluoro-elastomer (Solvay Solexis) was used as the continuous polymeric matrix and Asahiklin (AK225, Asahi Glass Company) was used as the solvent for the polymer and fluorodecyl POSS. Silicon wafers were coated with a POSS (50 % by weight) - Tecnoflon (50 % by weight) solution (total solids 10 mg/ml) or with a polyethyl methacrylate (PEMA) solution by spin-coating at 900 rpm for 30 seconds. Commercially available stainless steel woven meshes (McMaster-Carr) were used as model textured surfaces. These meshes were dip-coated in either a POSS (50%) – Tecnoflon (BR 9151, fluoro-elastomer from Solvay Solexis) (50%) solution or a polyethyl methacrylate (Aldrich, PEMA) solution with a total solid concentration of 10 mg/ml. After immersion for 10 minutes, the dip-coated samples were removed and dried in a vacuum oven at 60°C for 30 minutes to ensure complete evaporation of the Asahiklin solvent.

Surface characterization – Contact angle measurements were performed using a VCA2000 goniometer (AST Inc.). Advancing and receding contact angles were measured with ~5 μL droplets of various liquids (purchased from Aldrich and used as received). JEOL 6060 scanning electron microscope was used at an acceleration voltage of 3 kV for taking SEM images of the dip-coated meshes.

Results and Discussion

Apparent contact angles on dip-coated carbon paper

To test the utility of the robustness factor framework, a commercially available cylindrically textured surface (carbon paper from Toray, Japan) was selected. It was dip-coated with a 50% POSS – 50% Tecnoflon solution and the apparent contact angle was measured using various test liquids. In our previous work,[25] we demonstrated that the effective spacing ratio (D^*) is readily obtained by fitting the CB relation (Equation (1)) to contact angle data plotted as ($\cos\theta^*_{adv}$ vs $\cos\theta_{adv}$). Using the value of the spacing ratio (D^*) determined from this fit, the dimensionless robustness factor (A^*, Equation (2)) can

also be plotted on the same non-wetting diagram, and the magnitude of the robustness factor helps to rationalize the transition from the composite to the fully-wetted interface. For the carbon paper example in Figure 1, the spacing ratio for the carbon paper was computed to be $D^* = 4.1 \pm 0.6$ from regression to the measured advancing contact angle data on the textured (θ^*_{adv}) and smooth surface (θ_{adv}).[25] The coated surface is superhydrophobic with $\theta^*_{adv} = 153 \pm 2°$ for water droplets. Liquids like methanol ($\gamma_{lv} = 22.7$ mN/m, $\theta_{adv} = 55 \pm 3°$, $\theta^*_{adv} = 120 \pm 3°$, $A^* = 8.1$) and octane ($\gamma_{lv} = 21.6$ mN/m, $\theta_{adv} = 51 \pm 3°$, $\theta^*_{adv} = 106 \pm 3°$, $A^* = 6.9$) also formed robust composite interfaces on the dip-coated carbon paper ($R = 6$ μm, $D^* = 4.1 \pm 0.6$). On the contrary, heptane ($\gamma_{lv} = 20.1$ mN/m, $\theta_{adv} = 45 \pm 3°$, $\theta^*_{adv} \approx 0°$, $A^* = 5.8$) wetted the textured surface. The observed spontaneous wetting by heptane was not expected because according to the design parameter framework, the solid-liquid-air composite interface is robust for all values of $A^* > 1$. Although the trend of decreasing apparent contact angle and robustness measurements with changes in γ_{lv} is qualitatively correct, it is clear that the criterion is not a quantitative predictor of the crossover from a Cassie-Baxter[21] (composite interface) to a Wenzel[37] (fully wetted) state. From the SEM micrograph of the carbon paper surface, it is clear that the individual fibers forming the re-entrant texture are distributed randomly and there is a considerable local variation in the value of D^*. Therefore the carbon paper surface or any other nonwoven fiber mat surface with a broad variation in the surface topography is not suitable for quantitative analysis of the effect of varying topographical and surface properties on liquid non-wettability and robustness. Consequently, in the following sections we turn to a series of woven meshes, each with regular periodic texture, as the model textured surfaces.

Contact angle measurements on dip-coated woven meshes

The woven meshes offer a set of periodic textured surfaces which are commercially available. The mesh number refers to the number of openings per inch, therefore a smaller mesh number indicates a coarse mesh and a larger mesh number indicates a finer mesh. The influence of chemical interaction between various liquids and coating materials (θ_E), the characteristic cylinder length scale (R), and the

spacing between cylindrical fibers (D^*) on the wettability (θ^*) and robustness (A^*) can be systematically evaluated by measuring the apparent contact angles on woven meshes with a variety of coatings, wire radii, and spacing ratios respectively. In the first set of experiments, three wire meshes (mesh 50 with R = 114 μm, mesh 100 with R = 57 μm and mesh 325 with R = 18 μm) with identical spacing ratio (D^* = 2.2) were selected. These wire meshes were each dip-coated using different solutions with a range of solid surface energies (γ_{sv}): (i) a 50/50 (by weight) mixture of fluorodecyl POSS and Tecnoflon (BR 9151, a fluoroelastomer from Solvay-Solexis), (ii) pure Tecnoflon and (iii) polyethyl methacrylate (PEMA). The solid surface energies (γ_{sv}) of (i) 10.7, (ii) 18.3 and (iii) 32.2 mN/m were estimated using the Owens-Wendt analysis with water and octane as the probing liquids.[38] Different polar liquids (water (γ_{lv} = 72.1 mN/m), ethylene glycol (γ_{lv} = 47.7 mN/m), and methanol (γ_{lv} = 22.7 mN/m)), non-polar liquids (methylene iodide (γ_{lv} = 50.8 mN/m) and rapeseed oil (γ_{lv} = 35.5 mN/m) in addition to a homologous series of n-alkanes starting from hexadecane (γ_{lv} = 27.5 mN/m) to pentane (γ_{lv} = 15.5 mN/m)) were used as contacting liquids for contact angle measurements. The advancing contact angle measurements on flat spin-coated silicon wafer surfaces (θ_{adv}) and the textured dip-coated mesh surfaces (θ^*_{adv}) can all be displayed in a compact manner on the generalized wetting diagram, as shown in Figure 2.

The spacing ratio (D^*) for the set of dip-coated meshes was estimated as 2.45 ± 0.2 by regression of the contact angle data[25] and this value of D^* compared favorably with the estimated value of the spacing ratio from the inspection of the SEM micrographs (D^* = 2.2, Figure 2). The CB relation (Equation (1)) is independent of the length scale of the surface features, therefore the apparent advancing contact angles (θ^*_{adv}) data on the dip-coated meshes (for R = 18, 57 and 114 μm) collapse onto a single curve corresponding to D^* = 2.45 ± 0.2 (Figure 2). The transition from a robust composite interface to a fully-wetted interface occurrs on all three meshes, but at different equilibrium contact angles. This mismatch in the equilibrium contact angle at which the failure of the composite interface occurs can be rationalized on the basis of the robustness factors for the dip-coated wire meshes. The robustness factor

(A^*, Equation (2)) varies inversely with the length-scale of the surface texture (R); the composite interface therefore fails at the highest equilibrium contact angle for the coarsest mesh ($\theta_{E,crit} \approx 42°$ for mesh 50, $R = 114$ μm) and at the lowest θ_E for the finest wire mesh ($\theta_{E,crit} \approx 14°$ for mesh 325, $R = 18$ μm). By implicitly solving Equation (2) with $A^* = 1$, values of for $\theta_{E,crit}$ are predicted to be 42, 27 and 14° respectively for the mesh 50, 100 and 325 surfaces. The generalized wetting diagram depicted in Figure 2 has been popularized by numerous groups and it has become an established paradigm to represent changes to the apparent contact angle (θ^*) data on textured surfaces in comparison to the equilibrium contact angle (θ_E) on chemically identical flat surface. [39-42] This framework indeed provides a compact way to represent data on self-similar structures, but the impact of individual parameters, namely the spacing ratio (D^*) and the length scale of the texture (R) on the non-wettability cannot be deconvoluted readily.

Design chart for liquid wettability on cylindrically textured surfaces

The two independent variables in the modified form of the CB relation (Equation (1)) are the equilibrium contact angle on a flat surface (θ_E) and the dimensionless spacing ratio (D^*). In order to mitigate the shortcomings of the generalized wetting diagram, a new design chart for understanding liquid wettability on omniphobic surfaces is proposed (Figure 3) in which the two independent variables are D^* and θ_E. The limiting values along the ordinate axis are chosen based on the accessible equilibrium contact angle values (θ_E) for water ($\gamma_{lv} = 72.1$ mN/m), from ~0° on a clean glass surface to ~125° on a pure fluorodecyl POSS surface.[6] On this design chart, the ordinate (θ_E) is uniquely determined by the chemistry of the solid coating and the contacting liquid. This variation in the inherent solid-liquid interactions is independent of the surface topography of a textured surface which is the geometrical spacing ratio (D^*) on the abscissa. The lower limit of the spacing ratio is chosen as the smallest physically possible value of $D^* = 1$ and the upper limit is arbitrarily chosen to be $D^* = 2\pi$ corresponding to a very open weave texture. Four contours of fixed apparent contact angle ($\theta^* = 0$, 90,

120 and 150°) are calculated from the CB relation (Equation (1)) and are plotted on this (D^*, θ_E) design space.

Cassie-Baxter used the apparent advancing (θ^*_{adv}) and receding contact angles (θ^*_{rec}) as the ordinate in their chart[21] whereas in the design chart presented here, the equilibrium contact angle on a chemically identical (θ_E) flat surface is plotted on the y-axis. The apparent advancing/receding contact angles are 'composite' variables that depend on chemistry, and the 'texture', (which consist of specific lithographic patterning, random roughness, weave/weft of woven structures etc). For this reason we argue that it is better to plot measured values of θ^* as a function of the two independent variables represented by the x and y axes. The important performance parameters (θ^* and A^*) of a coated fabric or other textured surfaces are then shown as contours of various constant value in our presentation, and they provide clear guidance for anticipating the efficacy of various designs that are based on selected values of D^* and θ_E. The equilibrium contact angle (θ^*) cannot be measured easily on textured surfaces, but it can be bracketed using the measured advancing and receding contact angles ($\theta^*_{adv} \geq \theta^* \geq \theta^*_{rec}$). Onda, Shibuichi and co-workers[39, 41, 42] report that the equilibrium contact angles are closer to the advancing contact angles than the receding contact angles. Therefore, in the design charts described below, we replace the equilibrium contact angle (θ_E) with the advancing contact angle on the flat surface (θ_{adv}) and the equilibrium contact angle on a textured surface (θ^*) with the apparent advancing contact angle (θ^*_{adv}).

As we have noted above, the apparent contact angle (θ^*) depends only on θ_E and D^* and it is independent of the length-scale (R) of the texture, which thus does not appear on the design chart. Consequently, while the design chart predicts the magnitude of the apparent contact angle (θ^*), it does not guarantee the existence or stability of the solid-liquid-air composite state. The graphical framework shown in Figure 3 does not recognize that the composite interface, needed to achieve high values of θ^*, may be metastable or completely unstable, nor does it quantify the magnitude of the breakthrough

pressure difference (P_b) required to disrupt a metastable composite (Cassie-Baxter) interface sufficiently to transition it to the fully-equilibrated wetted (Wenzel) state.

When represented on the design chart (Figure 3), the super-wetting region exists at the lower-left where the apparent contact angle predicted by the CB relation is nearly zero ($\theta^* \approx 0°$), even though the equilibrium contact angle on a chemically identical smooth surface is non-zero ($\theta_E > 0°$). This super-wetting region appears as a consequence of the cylindrical texture and in this region the additional energy released from the enhanced surface area provided by the texture coupled with the intrinsic partial wettability of the solid material results in complete wetting.[13, 42] From the design chart representation it is clear that the apparent contact angle (θ^*) can be increased by moving on the plot from left to right (by increasing D^*, the relative spacing of the topographical features) and/or by moving from bottom to top (by increasing θ_E which, for a selected liquid, is achieved through changes in the solid surface chemistry). The region bounded by the blue curve and the two axes (right top) is the region of super liquid non-wettability (*superhygrophobicity*)[4] characterized by a high value of apparent contact angle ($\theta^* > 150°$).

Incorporation of the robustness criterion on the design chart

Although this new design chart indicates the range of effective contact angles that can be achieved theoretically, it does not indicate if the resulting composite interface is stable. A modified form of the design chart for liquid wettability is presented in Figure 4. Here the shaded grey area represents combinations of the parameters θ_E, D^* and (ℓ_{cap} / R) for which the robustness factor is less than unity. The CB predictions (Equation (1)) are not extended into the shaded area as the composite interface becomes unstable; a liquid drop placed on the texture will spontaneously transition to a fully-wetted interface in this grey shaded region. Important to note that the amount of (white) area on this design chart, corresponding to regions in which liquid drops can be supported on a composite air-solid interface, can be tuned by varying the ratio ℓ_{cap} / R. The capillary length is a material property of the

contacting liquid ($\ell_{cap} = \sqrt{\gamma_{lv} / \rho g}$) and practical values span an approximate range from 2.7 mm for water (γ_{lv} = 72.1 mN/m, ρ = 1000 kg/m3) to 1.25 mm for methylene iodide (γ_{lv} = 50.8 mN/m, ρ = 3325 kg/m3); that is the range of values over which the capillary length can be varied is quite limited. On the contrary, the radius of the cylindrical re-entrant features (R) on the surface can be varied by many orders of magnitude ($R \approx 100$ μm for commercial fabrics down to $R \approx 100$ nm for electrospun mats). When droplets of a given liquid (with fixed ℓ_{cap}) are placed on a textured surface with a particular spacing ratio (fixed D^*) and a specific coating (fixed θ_E), both the robustness factor (A^*) and the breakthrough pressure (P_b) are inversely proportional to the surface texture length scale R. In the case of smaller length-scale surface features (small R, or large ℓ_{cap} / R), a large fraction of the θ_E and D^* parameter space corresponds to a robust composite interface ($A^* > 1$) and is available for the design of robust non-wettable surfaces. The variation in the accessible area for designing non-wetting surfaces is schematically shown in Figure 4 with two different feature sizes. [See supporting information for a video showing how the accessible area varies for designing non-wetting surfaces with the texture length scale.] The line corresponding to $A^* = 1$ (Equation (2)) varies with D^* and θ_E for $0.2 \leq \ell_{cap} / R \leq 2000$. By keeping the surface chemistry of the solid, the composition of the contacting liquid and the geometric spacing ratio the same (*i.e.* fixed θ_E and D^*), and only reducing the length scale of the surface texture (R), the anticipated wetting behavior for a liquid droplet on a textured surface can be controlled from a super-wetting state to a robust composite non-wetting state.

In the design chart framework presented here, the three main factors that govern the robustness of repellency to a selected liquid are completely decoupled: (i) the equilibrium contact angle exhibited by the liquid on a chemically identical smooth surface (θ_E), (ii) the spacing ratio of the textured surface (D^*), and (iii) the length scale of the features that produce the surface texture (R). It is straightforward to ascertain the effect of each one of these parameters on the robustness (A^*) and non-wettability (θ^*) of a textured surface, and it is clear that each of these parameters can be usefully manipulated during the

design process. Similar design charts can be developed for surfaces with other texture geometries (*e. g.* micro-hoodoos,[6] nano-nails[1] etc.) by modifying the expression for A^* (see supporting information) to account for the specific surface topography.

The main focus of the present manuscript is to elucidate the impact of the length scale (R), the spacing ratio D^* and surface chemistry (θ_E) on the apparent contact angle (θ^*) and the robustness (A^*) of the solid-liquid-air composite interface. Cassie and Baxter worked with similar textured surfaces but they were concerned only with the apparent contact angles (θ^*) and focused exclusively on water (γ_{lv} = 72.1 mN/m) as the probing liquid. In this work, liquids with a broad range of surface tensions (from 72.1 mN/m for water to 15.5 mN/m for pentane) are used in order to explore non-wettability of woven and nonwoven structures to a wide range of liquids.

Varying the length scale (R) at constant coating chemistry (θ_E) and spacing ratio (D^*)

The effect of the microscopic length scale of the surface texture on the robustness of the composite interface is elucidated more clearly with the help of the design chart developed in this work. Figure 5 shows contact angle data measured on two 50% POSS – 50% Tecnoflon coated woven surfaces – mesh 325 (R = 18 μm, D^* = 2.45 ± 0.2, Figure 5(a)) and mesh 50 (R = 114 μm, D^* = 2.45 ± 0.2, Figure 5(b)). Filled symbols on the design chart denote a robust composite interface whereas open symbols indicate a fully-wetted interface on the textured mesh surface. The liquid alkane with the lowest surface tension *i.e.* pentane (⬟ in Figure 5(a), γ_{lv} = 15.5 mN/m) formed a robust composite non-wetting interface (with θ^*_{adv} = 91 ± 3°) on the finest mesh (325) dip-coated with 50% POSS – 50% Tecnoflon. On the contrary, even relatively higher tension liquids such as heptane (☆ in Figure 5(b), γ_{lv} = 20.1 mN/m, θ_{adv} = 45 ± 2°) and pentane (⬠ in Figure 5(b), γ_{lv} = 15.5 mN/m, θ_{adv} = 35 ± 3°) wet the identically coated textured surface (resulting in $\theta^*_{adv} \approx 0°$) of mesh 50. Although both the textured surfaces have identical coating chemistry, their different characteristic length scales result in different robustness factors. The value of A^* is reduced from high values at fine length scale *i.e.* A^*_{pentane} = 5.8 and A^*_{heptane} = 9.1 on mesh

325 ($R = 18$ μm), to lower values at a coarser length scale *i.e.* $A^*_{\text{pentane}} = 0.9$ and $A^*_{\text{heptane}} = 1.4$ ($R = 114$ μm). When the robustness factor reaches a value close to unity ($A^* \lesssim 1$), the composite interface sags severely and touches the next underlying layer of the solid texture, which results in a transition to the fully-wetted state. This transition is expected to take place at values of A^* order unity. In our idealized model (*i.e.* a periodic array of parallel cylinders), we expect $A^*_{crit} = 1$ and indeed our observations suggest that the critical robustness factor is always $1 < A^*_{crit} < 1.5$. For a comparatively higher surface tension liquid such as octane (■, $\gamma_{lv} = 21.6$ mN/m, $\theta_{adv} = 51 \pm 2°$), the robustness factor decreases from A^*_{octane}=11.2 on mesh 325 to A^*_{octane}=1.7 on mesh 50. Because the robustness factor remains sufficiently greater than unity, a robust composite non-wetting interface is observed for octane droplets on both the fine mesh 325 (θ^*_{adv}=109 ± 3°) and the coarse mesh 50 (θ^*_{adv}=107 ± 4°) provided they are dip-coated with 50% POSS – 50% Tecnoflon. Note that consistent with the length scale independence of Equation (1), the measured apparent advancing contact angles are essentially unaffected by the significant changes in R at constant D^*.

Varying the coating chemistry (θ_E) at constant spacing ratio (D^*) and length scale (R)

In addition to the length-scale of the texture, the robustness factor (A^*) also depends upon the equilibrium contact angle on a chemically identical smooth surface (θ_E). The impact of the variation in θ_E on the robustness factor (A^*) was studied by dip-coating wire mesh 325 ($R = 18$ μm, $D^* = 2.45 \pm 0.2$) using either a 50% POSS – 50% Tecnoflon ($\gamma_{sv} = 10.7$ mN/m, Figure 6(a)) or a polyethyl methacrylate (PEMA, $\gamma_{sv} = 32.2$ mN/m, Figure 6(b)) coating. For decane, the advancing contact angle on a smooth surfaces decreases from $\theta_{adv} = 60 \pm 2°$ on a flat 50% POSS – 50% Tecnoflon surface to $\theta_{adv} = 12 \pm 3°$ on a flat PEMA surface. The robustness factor decreases monotonically with θ_{adv}, from $A^*_{\text{decane}} = 14.6$ on mesh 325 ($R = 18$ μm) dip-coated with 50% POSS – 50% Tecnoflon to $A^*_{\text{decane}} = 0.8$ on the same woven surface coated with PEMA. As a result, decane forms a robust composite interface on mesh 325

($\theta^* = 108 \pm 3°$, ▼in Figure 6(a)) when it is coated with 50% POSS – 50% Tecnoflon but it fully wets the same underlying surface coated with PEMA ($\theta^* \approx 0°$, ▽in Figure 6(b)). By contrast, the advancing contact angle for dodecane (▲, $\gamma_{lv} = 25.3$ mN/m) changes from $\theta_{adv} = 71 \pm 2°$ to $19 \pm 2°$, and the robustness factor on the surface diminishes from 19 to 2.6. The robustness factor remains sufficiently greater than unity and a robust composite interface ($\theta^*_{adv} = 59 \pm 3°$,▲) is observed even on a PEMA coated mesh 325 surface. Hexadecane ($\gamma_{lv} = 27.5$ mN/m, $\theta_{adv} = 25 \pm 2°$, $A^* = 4.1$, $\theta^*_{adv} = 64 \pm 5°$) and dodecane ($\gamma_{lv} = 25.3$ mN/m, $\theta_{adv} = 19 \pm 2°$, $A^* = 2.6$, $\theta^*_{adv} = 59 \pm 3°$) form a robust metastable composite interface on a polyethyl methacrylate coated (PEMA, $\gamma_{sv} = 32.2$ mN/m) mesh 325 surface ($R = 18$ μm, $D^* = 2.45 \pm 0.2$). From the magnitude of A^*, the breakthrough pressure for hexadecane and dodecane droplets can be estimated to be about 118 and 71 Pa respectively. Also, the receding contact angles for hexadecane and dodecane droplets on the mentioned wire mesh surface were found to be close to zero.

These results illustrate that extremely low surface energy (γ_{sv}) coatings are not always necessary to obtain a robust composite interface provided the characteristic textural length scale is small enough. Even low surface tension liquids like hexadecane (⬣, $\gamma_{lv} = 27.5$ mN/m) and dodecane (▲, $\gamma_{lv} = 25.3$ mN/m) form robust and partially wetting composite interfaces ($\theta^*_{adv} = 64 \pm 5°$ for hexadecane and $\theta^*_{adv} = 59 \pm 3°$ for dodecane) on PEMA-coated stainless steel meshes with sufficiently small wire radii (R). The systematic understanding provided by the design chart and the data reported in this work show that by properly tailoring the surface topographical parameters (R, D^*) and surface chemistry (θ_E) appropriately, a robust composite interface can be achieved for a suitably designed surface and liquid pair.

Varying the spacing ratio (D^*) at constant coating chemistry (θ_E) and length scale (R)

From the observations in previous sections, we saw the impact of variation in (i) ℓ_{cap} / R or (ii) θ_E on the robustness factor (A^*). The third important factor that alters the robustness is the 'openness of the weave' or the spacing ratio (D^*) of the surface texture. The dependence of the robustness factor on D^* is

explored by choosing a set of wire meshes which have identical radii ($R = 83$ μm) but different density weaves, and thus different spacing ratio ($D^* = 2.2$, 3.9 and 5.1). These wire meshes are dip-coated using the 50% POSS – 50% Tecnoflon solution and the contact angle measurement results are plotted in Figure 7. For the wire mesh with the tightest weave *i.e.* the smallest spacing ratio ($D^* = 2.2$, $R = 83$ μm, mesh 70), liquids such as octane (■, $\gamma_{lv} = 21.6$ mN/m, $A^* = 2.4$, $\theta^* = 110 \pm 3°$), and heptane (★, $\gamma_{lv} = 20.1$ mN/m, $A^* = 1.9$, $\theta^* = 104 \pm 4°$) form a robust composite interface. On the contrary, pentane (⬠, $\gamma_{lv} = 15.5$ mN/m) readily wets this surface because the robustness factor approaches unity ($A^* = 1.2$, $\theta^* \approx 0°$). Dodecane (▲, $\gamma_{lv} = 25.3$ mN/m, $\theta^* = 123 \pm 3°$) forms a robust composite interface on the dip-coated mesh 70 surface ($R = 83$ μm, $D^* = 2.2$) whereas it wets an identically coated mesh 40 surface with a looser weave ($R = 83$ μm, $D^* = 3.9$, $\theta^* \approx 0°$, △). As feature spacing increases from 2.2 to 3.9, the spacing between the cylindrical texture increases (from $2D = 200$ to 470 μm) whereas the radius of the individual filament remains constant (at $R = 83$ μm). Consequently as D^* increases, the air-liquid interface sags more severely and the robustness factor decreases. For dodecane the robustness factor decreases from $A^* = 4.0$ to $A^* = 1.1$ as D^* increases from 2.2 to 3.9 at constant $R = 83$ μm and $\theta_{adv} = 71 \pm 2°$. Similarly, the robustness factor continues to decline in magnitude as the spacing ratio increases from $D^* = 3.9$ to $D^* = 5.1$. In the case of rapeseed oil (▶, $\gamma_{lv} = 35.5$ mN/m), the robustness factor decreases from $A^* = 1.6$ on mesh 40 surface down to $A^* = 0.9$ on mesh 30 surface (with $R = 83$ μm and $D^* = 5.1$). Consequently, as expected rapeseed oil wets the 50% POSS – 50% Tecnoflon coated mesh 30 surface (▷ for $R = 83$ μm and $D^* = 5.1$, $\theta^* \approx 0°$). Droplets of water ($\gamma_{lv} = 72.1$ mN/m, blue) and rapeseed oil ($\gamma_{lv} = 35.5$ mN/m, red) on (i) mesh 70 surface with $D^* = 2.2$, $R = 83$ μm and (ii) mesh 30 surface with $D^* = 5.1$ and $R = 83$ μm are shown in the inset of Figure 7. The figure illustrates the importance of the mesh weave and spacing ratio (D^*) on the robustness of the composite interface. The apparent contact angle (θ^*) increases monotonically with increasing spacing ratio (D^*), as the wetted fraction of the solid ($r_f \phi_s = (\pi - \theta_E) / D^*$) diminishes. As a result, provided a robust composite interface

is ensured ($A^* > 1$) then the apparent contact angle of water droplets ($\gamma_{lv} = 72.1$ mN/m, $\theta_{adv} = 122 \pm 2°$), increases from $\theta^* = 147 \pm 2°$ on mesh 70 ($R = 83$ μm, $D^* = 2.2$) to $\theta^* = 160 \pm 3°$ on mesh 30 (with $R = 83$ μm and $D^* = 5.1$). However if the robustness factor decreases below unity due to increasing spacing ratio (D^*), then the liquid droplets transition from a robust composite interface with high apparent contact angles to a fully wetted interface with very low apparent contact angles ($\theta^* \approx 0°$),[26] as in the case for decane droplets.

Incorporation of the thermodynamic equilibrium condition to the design chart

All the data presented above demonstrate the influence of the surface texture (R, D^*), the liquid parameters (ℓ_{cap}), and the solid surface chemistry (θ_E) on the robustness factor (A^*) for liquid droplets with metastable composite interface.[8] So far the data and the design chart provide no information about the locus of other possible configurations such as the thermodynamic equilibrium state.[3, 4, 8, 43] The apparent contact angle (θ^*) for a liquid droplet in a composite (or Cassie-Baxter) state on a cylindrically textured surface is given by Equation (1). On the other hand, the apparent contact angle (θ^*) for a fully-wetted (Wenzel) liquid droplet is given by the Wenzel relation[37] $\cos\theta^* = r\cos\theta_E$, where r is the Wenzel roughness given by the actual solid-liquid interfacial area divided by the projected solid-liquid interfacial area. For a parallel array of cylinders of radius R and spacing $2D$, the Wenzel roughness is $r = 1 + \pi/D^*$, where D^* is the spacing ratio. The condition for crossover to a thermodynamic equilibrium can be obtained by solving both the CB and the Wenzel relation simultaneously for the critical angle θ_c (Equation (3)).[4, 12, 44] This condition is plotted as the black dashed line on the design chart in Figure 8.

$$D^* = \frac{\sin\theta_c - \theta_c\cos\theta_c}{1 + \cos\theta_c} \qquad (3)$$

From Figure 8, it is clear that $\theta_E > 90°$ is a necessary condition for the existence of a truly thermodynamically stable composite interface. Because there is no natural or artificial surface with $\theta_E > 90°$ for liquids with low surface tension, the composite interfaces for such liquids are at best

metastable. Within the design chart represented by Figure 8, the region above the black dashed line corresponds to non-wetting droplets where the composite interface is the global minimum in free energy. This region is accessible essentially only with water (γ_{lv} = 72.1 mN/m) and other high surface tension liquids like glycerol (γ_{lv} = 64 mN/m), ethylene glycol (γ_{lv} = 47.7 mN/m) and methylene iodide (γ_{lv} = 50.8 mN/m). On the other hand, below the dashed line the fully-wetted or Wenzel state is the thermodynamic equilibrium and a composite interface (Cassie-Baxter) is, at best, metastable.[2, 5-7, 12, 27, 44-47] The cross-over condition from the Cassie-Baxter to Wenzel state is analogous to the binodal or the coexistence curve on a phase diagram.[48] Below this binodal curve, the composite interface is metastable but can still be realized under carefully controlled conditions until the necessary breakthrough pressure for the transition is applied (analogous to a nucleation event and the growth of the nucleus to reach the critical size). It is important to remember that the thermodynamic crossover condition is independent of the length scale of the texture (R), as Equation (3) is scale invariant.

The metastable region extends from the crossover condition (black dashed line) to the edge of the shaded region, where the composite interface is thermodynamically unstable ($A^* \lesssim 1$) and it spontaneously transitions into the fully-wetted interface. This transformation of the sagging liquid-air composite interface to a fully-wetted interface is analogous to a pseudo-spinodal on the phase diagram. At the pseudo-spinodal, an infinitesimally small external perturbation results in the spontaneous transformation (analogous to a spinodal decomposition which is spontaneous and has no nucleation events.) The pseudo-spinodal curve for the robust metastable regime found by setting $A^* = 1$ is a strong function of the length scale (R) (Equation (2), Figure 4 and Figure S3).

Conclusions

In the present work, we have presented a design chart to assist in the *a priori* prediction of the liquid wettability (θ^*) and the robustness factor (A^*) against wetting by a specified liquid on cylindrically textured surfaces. This design chart can be used to predict the existence of a robust composite (or

Cassie-Baxter) interface for a given combination of the relevant surface texture parameters, specifically the spacing ratio (D^*) and the length scale (R) of the surface texture; the equilibrium contact angle on a chemically equivalent smooth surface (θ_E) and the physical properties of the contacting liquid (ℓ_{cap}). To illustrate the utility of the design chart, we used a model system of woven meshes with an idealized periodic cylindrical texture. The physico-chemical parameters were systematically varied over wide ranges (18 μm $\leq R \leq$ 114 μm, 78° $\leq \theta_E \leq$ 122° (for water) and 2.2 $\leq D^* \leq$ 5.1) and their impact on both the robustness (A^*) and the level of non-wettability (θ^*) was assessed. As expected, the robustness of the resulting model surfaces (A^*) was found to be inversely proportional to the length scale of the surface texture ($A^* \propto 1/R$) and monotonically increased with increase of the equilibrium contact angle (θ_E) or decrease in spacing ratio (D^*) between the re-entrant features. We have focused on developing a design chart for cylindrically textured surfaces, but similar design charts can be developed for any other periodic texture such as a surface decorated with an array of spheres (see supporting information). Therefore the design chart provides a generic engineering and design framework to understand the wettability of textured surfaces.

ACKNOWLEDGMENT

This research was supported by the Army Research Office (ARO) through contract no. W911NF-07-D-0004 and the Air Force Research Lab (AFRL) under contract no. FA9300-06M-T015 and the Air Force Office of Scientific Research (AFOSR) under contract no. FA9550-07-1-0272 and LRIR-92PL0COR. We thank Prof. Michael Rubner and the Institute of Soldier Nanotechnologies (ISN) at MIT for the use of various experimental facilities and Mr. Abhinav Akhoury for the carbon paper sample.

SUPPORTING INFORMATION PARAGRAPH

The supporting information provides detailed explanation about (1) Design chart for liquid wettability on post-like texture, (2) Rationale for using the CB relation for the design chart and derivation of a model for the prediction of apparent advancing and receding contact angles, (3) Variation of the robustness factor on the design chart (4) Design chart for a surface textured with spheres of radius R and spacing $2D$, (5) Importance of the capillary length (ℓ_{cap}) and (6) Design chart for a dual-scaled textured surfaces. This material is available free of charge via the Internet at http://pubs.acs.org.

FIGURE CAPTIONS

Figure 1. (a) SEM image of the microfiber carbon paper (Toray, Japan) dip-coated with 50% POSS – 50% Tecnoflon. (b) Generalized wetting diagram for a 50 % POSS – 50% Tecnoflon (γ_{sv} = 10.7 mN/m) coated carbon paper. Apparent advancing contact angle data is plotted using water (●, γ_{lv} = 72.1 mN/m), rapeseed oil (▶, γ_{lv} = 35.5 mN/m), hexadecane (⬣, γ_{lv} = 27.5 mN/m), dodecane (▲, γ_{lv} = 25.3 mN/m), decane (▼, γ_{lv} = 23.8 mN/m), methanol (◆, γ_{lv} = 22.7 mN/m), octane (■, γ_{lv} = 21.6 mN/m), and heptane (☆, γ_{lv} = 20.1 mN/m). The spacing ratio is found to be D^* = 4.1 ± 0.6 from the regression of the CB relation (Equation (1)) to the contact angle data and the robustness factor is computed using this value of the D^* (Equation (2)).

Figure 2. Generalized non-wetting diagram for the dip-coated woven meshes. The cosine of the advancing contact angle on the textured dip-coated mesh surfaces (θ^*_{adv}) is plotted against the cosine of the advancing contact angle on the flat spin-coated silicon wafer surfaces (θ_{adv}). The data plotted on the non-wetting diagram is for three mesh sizes (mesh 50 with R = 114 μm (■), mesh 100 with R = 57 μm (●), mesh 325 with R = 18 μm (▲)) with three different coatings ((i) 50% fluorodecyl POSS – 50% Tecnoflon (γ_{sv} = 10.7 mN/m), (ii) Tecnoflon (γ_{sv} = 18.3 mN/m) and (iii) polyethyl methacrylate (PEMA)

(γ_{sv} = 32.2 mN/m)) and using various polar and non-polar liquids. The three arrows correspond to the values of $\theta_{E,\,crit}$ = 42, 27 and 14° for mesh 50, 100 and 325 respectively.

Figure 3. Design chart for liquid wettability on cylindrically textured surface. The contours of the apparent contact angle (θ^*) for (θ^* = 0 (—), 90 (—), 120 (—) and 150° (—)) are plotted on the design chart with the equilibrium contact angle on a chemically identical smooth surface (θ_E) and the spacing ratio (D^*) as the two axes. Various regimes of wettability starting from super-wetting ($\theta^* \approx 0°$) to super-nonwetting ($\theta^* > 150°$) are shown on the design chart.

Figure 4. Modified form of the design chart for liquid wettability, which predicts the parameter space available for designing robust composite interfaces for two values of the ratio (ℓ_{cap} / R). Figure 4(a) represents a typical commercial textile surface with $\ell_{cap} \approx 2$ mm, $R \approx 200$ μm, and $\ell_{cap} / R = 10$ and Figure 4(b) shows the modified design chart for a typical electrospun mat with $\ell_{cap} \approx 2$ mm, $R \approx 2$ μm, and $\ell_{cap} / R = 1000$.

Figure 5. Contact angle data on wire meshes dip-coated with 50% POSS – 50% Tecnoflon (γ_{sv} = 10.7 mN/m) using water (●, γ_{lv} = 72.1 mN/m), rapeseed oil (▶, γ_{lv} = 35.5 mN/m), hexadecane (⬢, γ_{lv} = 27.5 mN/m), dodecane (▲, γ_{lv} = 25.3 mN/m), decane (▼, γ_{lv} = 23.8 mN/m), methanol (◆, γ_{lv} = 22.7 mN/m), octane (■, γ_{lv} = 21.6 mN/m), heptane (☆, γ_{lv} = 20.1 mN/m), and pentane (⬟, γ_{lv} = 15.5 mN/m) are plotted on the design chart for liquid wettability. Figure 5(a) shows data for mesh 325 (R = 18 μm) and Figure 5(b) shows data for mesh 50 (R = 114 μm). The shaded area represents a set of (θ_E, D^*, ℓ_{cap}/R) values for which the robustness factor for heptane is less than unity ($A^*_{\text{heptane}} < 1$). Filled symbols indicate a liquid droplet with a robust composite interface whereas open symbols (☆,⬠ etc.) indicate a liquid droplet which has transitioned into the fully-wetted Wenzel state.

Figure 6. Contact angle data on the mesh 325 ($R = 18$ μm) using water (●, $\gamma_{lv} = 72.1$ mN/m), rapeseed oil (▶, $\gamma_{lv} = 35.5$ mN/m), hexadecane (⬢, $\gamma_{lv} = 27.5$ mN/m), dodecane (▲, $\gamma_{lv} = 25.3$ mN/m), decane (▼, $\gamma_{lv} = 23.8$ mN/m), methanol (◆, $\gamma_{lv} = 22.7$ mN/m), octane (■, $\gamma_{lv} = 21.6$ mN/m), heptane (☆, $\gamma_{lv} = 20.1$ mN/m), and pentane (⬟, $\gamma_{lv} = 15.5$ mN/m) are plotted on the design chart for liquid wettability. Figure 6(a) shows data for the mesh dip-coated with 50% POSS – 50% Tecnoflon ($\gamma_{sv} = 10.7$ mN/m) and Figure 6(b) shows data for the dip-coated mesh with PEMA ($\gamma_{sv} = 32.2$ mN/m). The shaded area represents a set of (θ_E, D^*, ℓ_{cap} / R) values for which the robustness factor for heptane is less than unity ($A^*_{\text{heptane}} < 1$). Because the characteristic length scale remains constant ($R = 18$ μm), the shaded area ($A^* < 1$, Equation (2)) remains the same in the two figures. Filled symbols indicate a liquid droplet with a robust composite interface whereas open symbols indicate a liquid droplet which has transitioned into the fully-wetted state.

Figure 7. Contact angle data on mesh 70, 40, and 30 (all with $R = 83$ μm and $D^* = 2.2$, 3.9, and 5.1 respectively) dip-coated using 50% POSS – 50% Tecnoflon. Contacting liquids include water (●, $\gamma_{lv} = 72.1$ mN/m), rapeseed oil (▶, $\gamma_{lv} = 35.5$ mN/m), hexadecane (⬢, $\gamma_{lv} = 27.5$ mN/m), dodecane (▲, $\gamma_{lv} = 25.3$ mN/m), decane (▼, $\gamma_{lv} = 23.8$ mN/m), methanol (◆, $\gamma_{lv} = 22.7$ mN/m), octane (■, $\gamma_{lv} = 21.6$ mN/m), heptane (☆, $\gamma_{lv} = 20.1$ mN/m), and pentane (⬟, $\gamma_{lv} = 15.5$ mN/m) are plotted on the design chart for liquid wettability. The shaded area represents a set of (θ_E, D^*, ℓ_{cap} / R) values for which the robustness factor for heptane is less than unity ($A^*_{\text{heptane}} < 1$). Filled symbols indicate a liquid droplet with a robust composite interface whereas open symbols indicate a liquid droplet which has transitioned into the fully-wetted interface. The left image in the inset shows nonwetting water (blue, $A^* = 14.5$) and rapeseed oil (red, $A^* = 5.8$) droplets with a robust composite interface on a mesh 70 surface ($R = 83$ μm; $D^* = 2.2$) coated with 50% POSS – 50% Tecnoflon. The right image shows a water droplet (blue, $A^* = 2.1$) in a robust composite interface on a mesh 30 ($R = 83$ μm and $D^* = 5.1$) surface with a similar

coating. Rapeseed oil (red) wets the textured surface because the robustness factor drops to $A^* = 0.9$. The SEM micrographs of the three textured surfaces are shown on the right.

Figure 8. The thermodynamic condition for cross-over from the composite to the fully-wetted interface is shown as the black dashed line on the design chart for liquid wettability. The shaded region indicates parameter space inaccessible for designing non-wetting surfaces with cylindrical textures of length scale R such that $\ell_{cap} / R = 100$.

REFERENCES

1. Ahuja, A.; Taylor, J. A.; Lifton, V.; Sidorenko, A. A.; Salamon, T. R.; Lobaton, E. J.; Kolodner, P.; Krupenkin, T. N., *Langmuir* **2008,** 24, 9-14.
2. Cao, L.; Price, T. P.; Weiss, M.; Gao, D., *Langmuir* **2008,** 24, 1640-1643.
3. Marmur, A., *Langmuir* **2003,** 19, 8343-8348.
4. Marmur, A., *Langmuir* **2008,** 24, 7573-7579.
5. Nosonovsky, M., *Langmuir* **2007,** 23, 3157-3161.
6. Tuteja, A.; Choi, W.; Ma, M.; Mabry, J. M.; Mazzella, S. A.; Rutledge, G. C.; McKinley, G. H.; Cohen, R. E., *Science* **2007,** 318, 1618-1622.
7. Tuteja, A.; Choi, W.; Mabry, J. M.; McKinley, G. H.; Cohen, R. E., *Proc. Natl. Acad. Sci. USA* **2008**, 18200-18205.
8. Tuteja, A.; Choi, W.; McKinley, G. H.; Cohen, R. E.; Rubner, M. F., *MRS Bull.* **2008,** 33, 752-758.
9. Brewer, S. A.; Willis, C. R., *Appl. Surf. Sci.* **2008,** 254, 6450-6454.
10. Ma, M.; Mao, Y.; Gupta, M.; Gleason, K. K.; Rutledge, G. C., *Macromolecules* **2005,** 38, 9742-9748.
11. He, B.; Patankar, N. A.; Lee, J., *Langmuir* **2003,** 19, 4999-5003.
12. Lafuma, A.; Quéré, D., *Nat Mater* **2003,** 2, 457-460.
13. McHale, G.; Shirtcliffe, N. J.; Aqil, S.; Perry, C. C.; Newton, M. I., *Phys. Rev. Lett.* **2004,** 93, 036102.
14. Quéré, D., *Physica A* **2002,** 313, 32-46.
15. Marmur, A., *Ann. Rev. Mater. Res.* **2009,** 39, 473-489.
16. Tsujii, K.; Yamamoto, T.; Onda, T.; Shibuichi, S., *Angew. Chem.* **1997,** 36, 1011-1012.
17. Shibuichi, S.; Yamamoto, T.; Onda, T.; Tsujii, K., *J. Colloid Interface Sci.* **1998,** 208, 287-294.
18. Gao, L.; McCarthy, T. J., *Langmuir* **2006,** 22, 2966-2967.
19. Shuttleworth, R.; Bailey, G. L. J., *Discuss Faraday Soc* **1948,** 3, 16-22.
20. Patankar, N. A., *Langmuir* **2004,** 20, 8209-8213.

21. Cassie, A.; Baxter, S., *T. Faraday Soc.* **1944,** 40, 546-551.
22. Kawase, T.; Fujii, T.; Minagawa, M., *Textile Research Journal* **1987,** 57, 185-191.
23. Michielsen, S.; Lee, H. J., *Langmuir* **2007,** 23, 6004-6010.
24. Nosonovsky, M.; Bhushan, B., *Langmuir* **2008,** 24, 1525-1533.
25. Chhatre, S. S.; Tuteja, A.; Choi, W.; Revaux, A.; Smith, D.; Mabry, J. M.; McKinley, G. H.; Cohen, R. E., *Langmuir* **2009,** In Press.
26. Choi, W.; Tuteja, A.; Chhatre, S.; Mabry, J. M.; Cohen, R. E.; McKinley, G. H., *Adv. Mater.* **2009,** 21, 2190-2195.
27. Cao, L.; Hu, H.; Gao, D., *Langmuir* **2007,** 23, 4310-4314.
28. Young, T., *Philos. Trans. R. Soc. London* **1805,** 95, 65-87.
29. Choi, W.; Tuteja, A.; Mabry, J. M.; Cohen, R. E.; McKinley, G. H., *J. Colloid Interface Sci.* **2009,** 339, 208-216.
30. Ma, M.; Hill, R. M.; Rutledge, G. C., *J. Adhes. Sci. Technol.* **2008,** 22, 1799-1817.
31. Gao, L.; McCarthy, T. J., *Langmuir* **2006,** 22, 5998-6000.
32. Hoefnagels, H. F.; Wu, D.; deWith, G.; Ming, W., *Langmuir* **2007,** 23, 13158-13163.
33. Leng, B.; Shao, Z.; de With, G.; Ming, W., *Langmuir* **2009,** 25, 2456-2460.
34. Han, D.; Steckl, A. J., *Langmuir* **2009,** In Press.
35. Aussillous, P.; Quéré, D., *Proc. R. Soc. A-Math. Phy.* **2006,** 462, 973-999.
36. Mabry, J.; Vij, A.; Iacono, S.; Viers, B., *Angew. Chem. Int. Ed.* **2008,** 47, 4137-4140.
37. Wenzel, R. N., *Ind. Eng. Chem.* **1936,** 28, 988-994.
38. Owens, D. K.; Wendt, R. C., *J. Appl. Polym. Sci.* **1969,** 13, 1741-1747.
39. Onda, T.; Shibuichi, S.; Satoh, N.; Tsujii, K., *Langmuir* **1996,** 12, 2125-2127.
40. Quéré, D., *Rep. Prog. Phys.* **2005**, 2495.
41. Shibuichi, S.; Onda, T.; Satoh, N.; Tsujii, K., *J. Phys. Chem.* **1996,** 100, 19512-19517.
42. Quéré, D., *Ann. Rev. Mater. Res.* **2008,** 38, 71-99.
43. Patankar, N. A., *Langmuir* **2004,** 20, 7097-7102.
44. Barbieri, L.; Wagner, E.; Hoffmann, P., *Langmuir* **2007,** 23, 1723-1734.
45. Herminghaus, S., *Europhys. Lett.* **2000,** 52, 165.
46. Jian-Lin, L.; Xi-Qiao, F.; Gangfeng, W.; Shou-Wen, Y., *J. Phys.: Condens. Matter* **2007,** 19, 356002.
47. Kurogi, K.; Yan, H.; Tsujii, K., *Colloids Surf. Physicochem. Eng. Aspects* **2008,** 317, 592-597.
48. Tester, J. W.; Modell, M., *Thermodynamics and Its Applications (3rd Edition)*. Prentice Hall PTR: 1996; p 201-220.

SYNOPSIS TOC

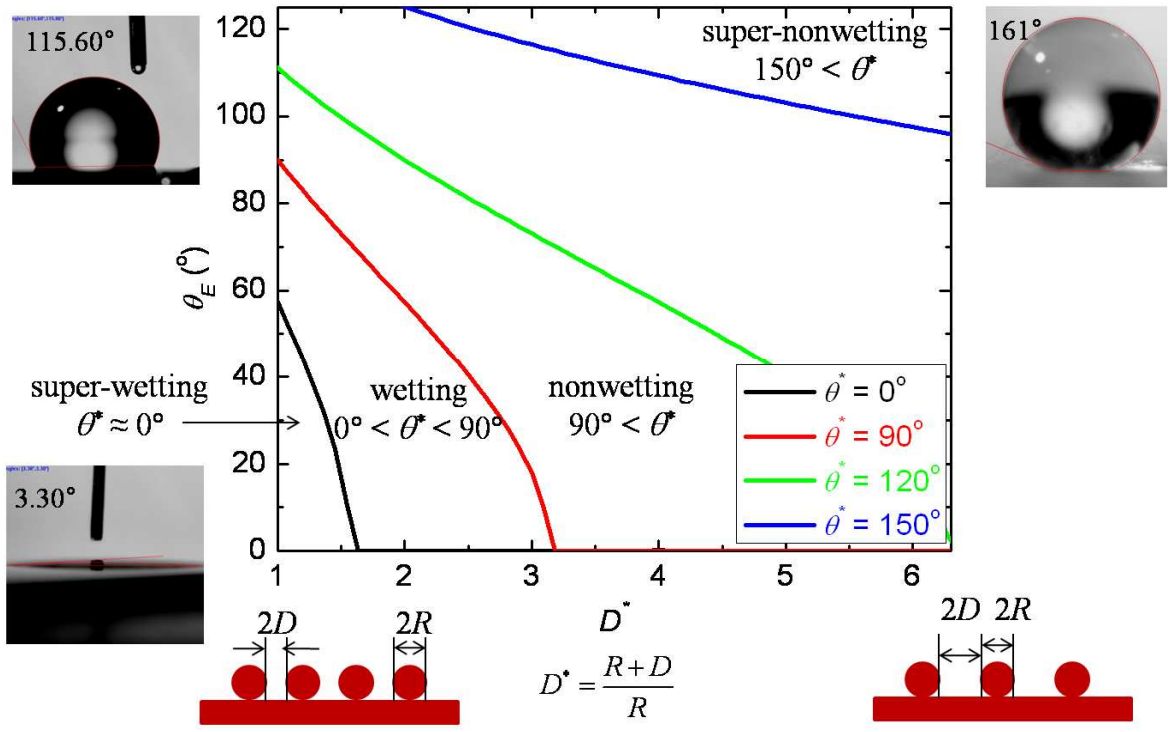

Design chart for liquid wettability on cylindrically textured surface. The contours of the apparent contact angle (θ^*) for (θ^* = 0 (—), 90 (—), 120 (—) and 150° (—)) are plotted on the design chart with the equilibrium contact angle on a chemically identical smooth surface (θ_E) and the spacing ratio (D^*) as the two axes. Various regimes of wettability starting from super-wetting ($\theta^* \approx 0°$) to super-nonwetting ($\theta^* > 150°$) are shown on the design chart.

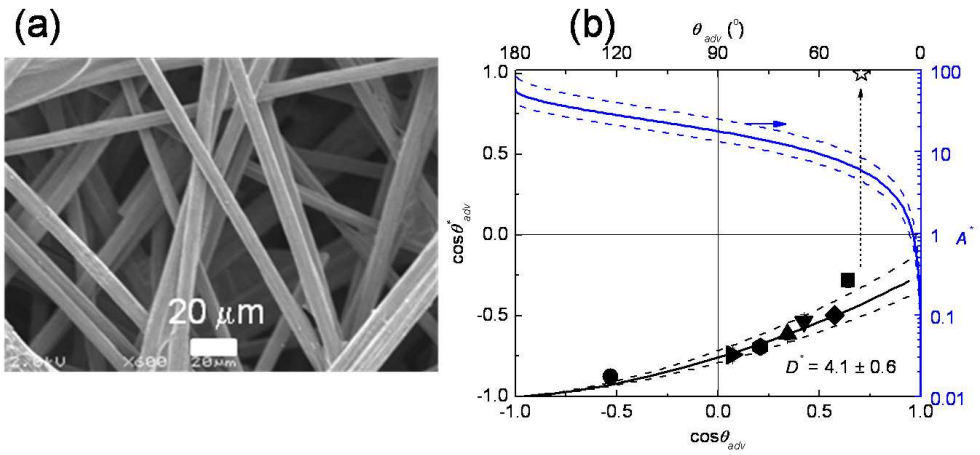

Figure 1. (a) SEM image of the microfiber carbon paper (Toray, Japan) dip-coated with 50% POSS – 50% Tecnoflon. (b) Generalized wetting diagram for a 50 % POSS – 50% Tecnoflon (γ_{sv} = 10.7 mN/m) coated carbon paper. Apparent advancing contact angle data is plotted using water (γ_{lv} = 72.1 mN/m), rapeseed oil (γ_{lv} = 35.5 mN/m), hexadecane (γ_{lv} = 27.5 mN/m), dodecane (γ_{lv} = 25.3 mN/m), decane (γ_{lv} = 23.5 mN/m), methanol (γ_{lv} = 22.7 mN/m), octane (γ_{lv} = 21.6 mN/m), and heptane (γ_{lv} = 20.1 mN/m). The spacing ratio is found to be D^* = 4.1 ± 0.6 from the regression of the CB relation (Equation (1)) to the contact angle data and the robustness factor is computed using this value of the D^* (Equation (2)).
233x105mm (150 x 150 DPI)

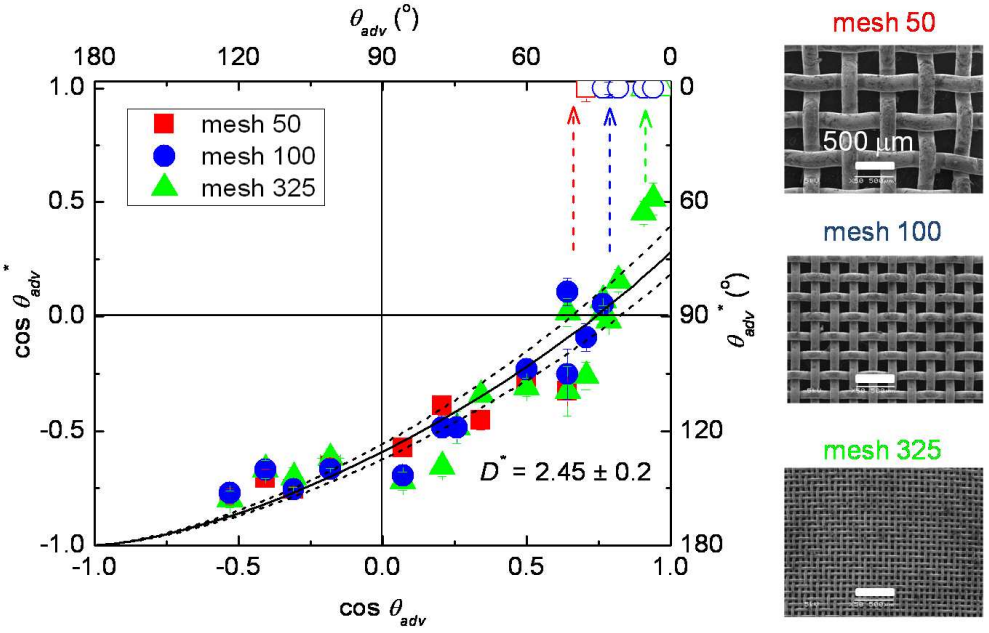

Figure 2. Generalized non-wetting diagram for the dip-coated woven meshes. The cosine of the advancing contact angle on the textured dip-coated mesh surfaces (θ^*_{adv}) is plotted against the cosine of the advancing contact angle on the flat spin-coated silicon wafer surfaces (θ_{adv}). The data plotted on the non-wetting diagram is for three mesh sizes (mesh 50 with R = 114 µm, mesh 100 with R = 57 µm, mesh 325 with R = 18 µm) with three different coatings ((i) 50% fluorodecyl POSS – 50% Tecnoflon (γ_{sv} = 10.7 mN/m), (ii) Tecnoflon (γ_{sv} = 18.3 mN/m) and (iii) polyethyl methacrylate (PEMA) (γ_{sv} = 32.2 mN/m)) and using various polar and non-polar liquids. The three arrows correspond to the values of $\theta_{E,\,crit}$ = 42, 27 and 14° for mesh 50, 100 and 325 respectively. 233x147mm (150 x 150 DPI)

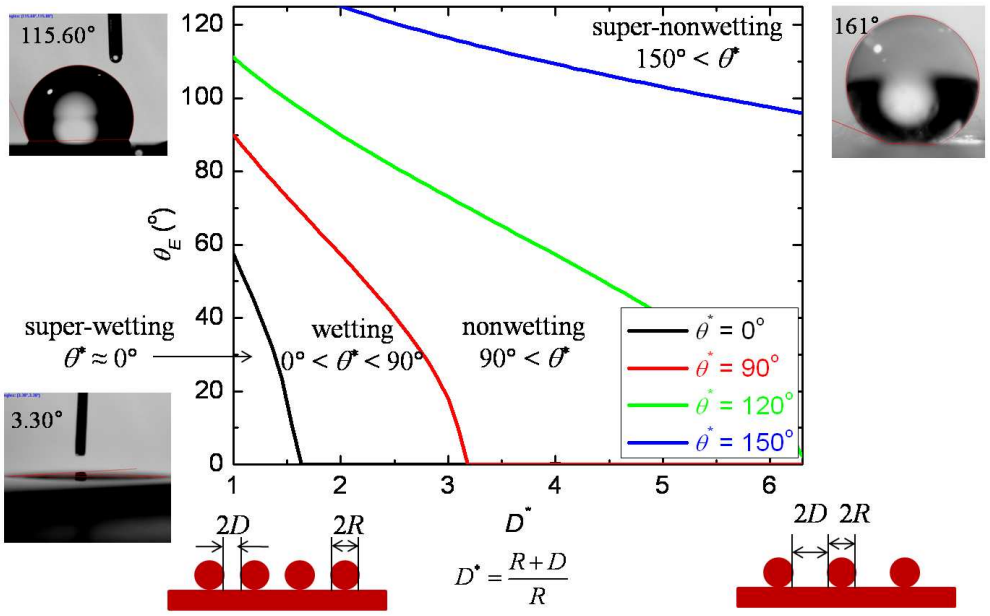

Figure 3. Design chart for liquid wettability on cylindrically textured surface. The contours of the apparent contact angle (θ^*) for (θ^* = 0, 90, 120 and 150°) are plotted on the design chart with the equilibrium contact angle on a chemically identical smooth surface (θ_E) and the spacing ratio (D^*) as the two axes. Various regimes of wettability starting from super-wetting ($\theta^* \approx 0°$) to super-nonwetting ($\theta^* > 150°$) are shown on the design chart.
234x147mm (150 x 150 DPI)

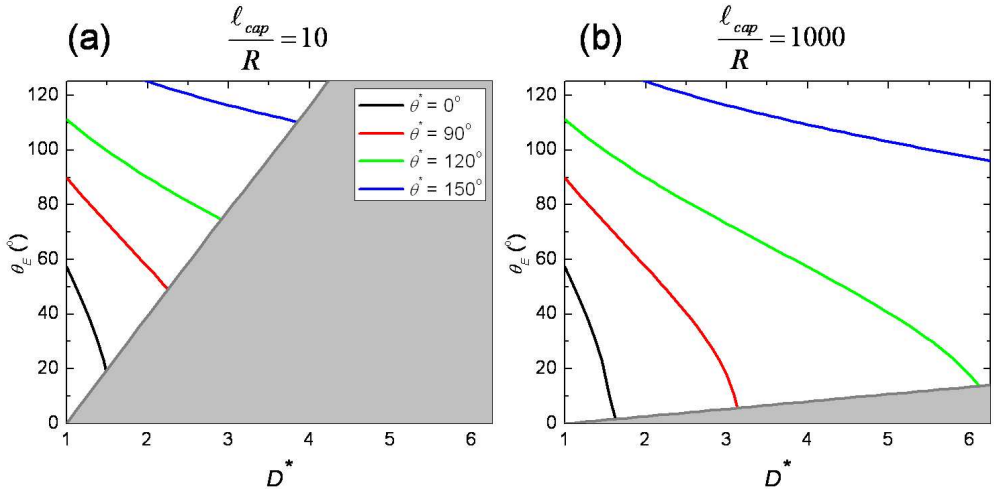

Figure 4. Modified form of the design chart for liquid wettability, which predicts the parameter space available for designing robust composite interfaces for two values of the ratio (l_{cap}/R). Figure 4(a) represents a typical commercial textile surface with $l_{cap} \approx$ 2 mm, $R \approx$ 200 μm, and l_{cap}/R= 10 and Figure 4(b) shows the modified design chart for a typical electrospun mat with $l_{cap} \approx$ 2 mm, $R \approx$ 2 μm, and l_{cap}/R= 1000.
252x124mm (150 x 150 DPI)

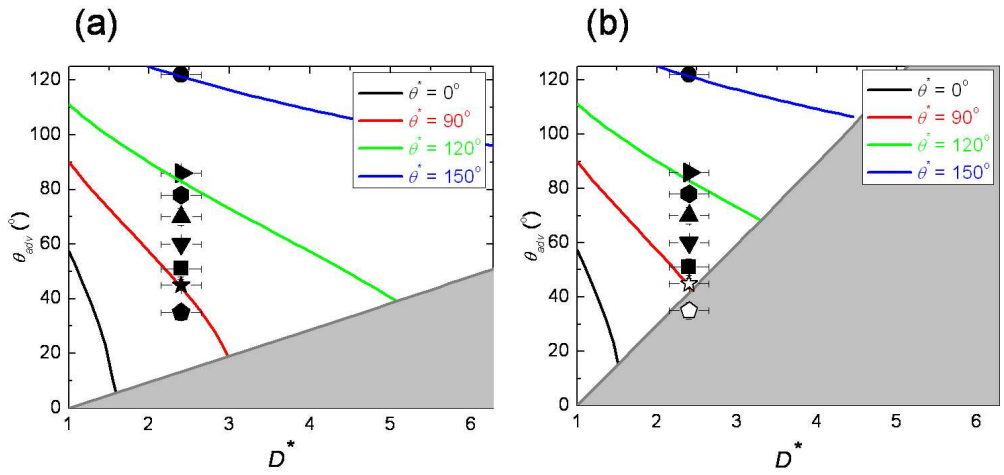

Figure 5. Contact angle data on wire meshes dip-coated with 50% POSS – 50% Tecnoflon (γ_{sv} = 10.7 mN/m) using water ((γ_{lv} = 72.1 mN/m), rapeseed oil (γ_{lv} = 35.5 mN/m), hexadecane (γ_{lv} = 27.5 mN/m), dodecane (γ_{lv} = 25.3 mN/m), decane (γ_{lv} = 23.8 mN/m), octane (γ_{lv} = 21.6 mN/m), heptane (γ_{lv} = 20.1 mN/m), and pentane (γ_{lv} = 15.5 mN/m) are plotted on the design chart for liquid wettability. Figure 5(a) shows data for mesh 325 (R = 18 μm) and Figure 5(b) shows data for mesh 50 (R = 114 μm). The shaded area represents a set of (θ_E, D^*, l_{cap}/R) values for which the robustness factor for heptane is less than unity ($A^*_{heptane}$ < 1). Filled symbols indicate a liquid droplet with a robust composite interface whereas open symbols indicate a liquid droplet which has transitioned into the fully-wetted Wenzel state.
252x121mm (150 x 150 DPI)

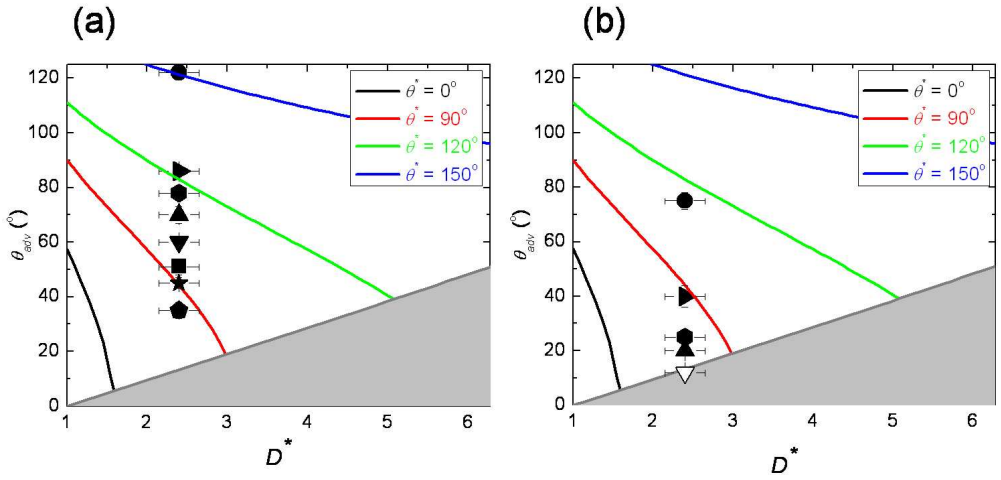

Figure 6. Contact angle data on the mesh using water ((γ_{lv} = 72.1 mN/m), rapeseed oil (γ_{lv} = 35.5 mN/m), hexadecane (γ_{lv} = 27.5 mN/m), dodecane (γ_{lv} = 25.3 mN/m), decane (γ_{lv} = 23.8 mN/m), octane (γ_{lv} = 21.6 mN/m), heptane (γ_{lv} = 20.1 mN/m), and pentane (γ_{lv} = 15.5 mN/m) are are plotted on the design chart for liquid wettability. Figure 6(a) shows data for the mesh dip-coated with 50% POSS – 50% Tecnoflon (γ_{sv} = 10.7 mN/m) and Figure 6(b) shows data for the dip-coated mesh with PEMA (γ_{sv} = 32.2 mN/m). The shaded area represents a set of (θ_E, D^*, l_{cap}/R) values for which the robustness factor for heptane is less than unity ($A^*_{heptane}$ < 1). Because the characteristic length scale remains constant (R = 18 μm), the shaded area (($A^*_{heptane}$ < 1, Equation (2)) remains the same in the two figures. Filled symbols indicate a liquid droplet with a robust composite interface whereas open symbols indicate a liquid droplet which has transitioned into the fully-wetted state.
253x121mm (150 x 150 DPI)

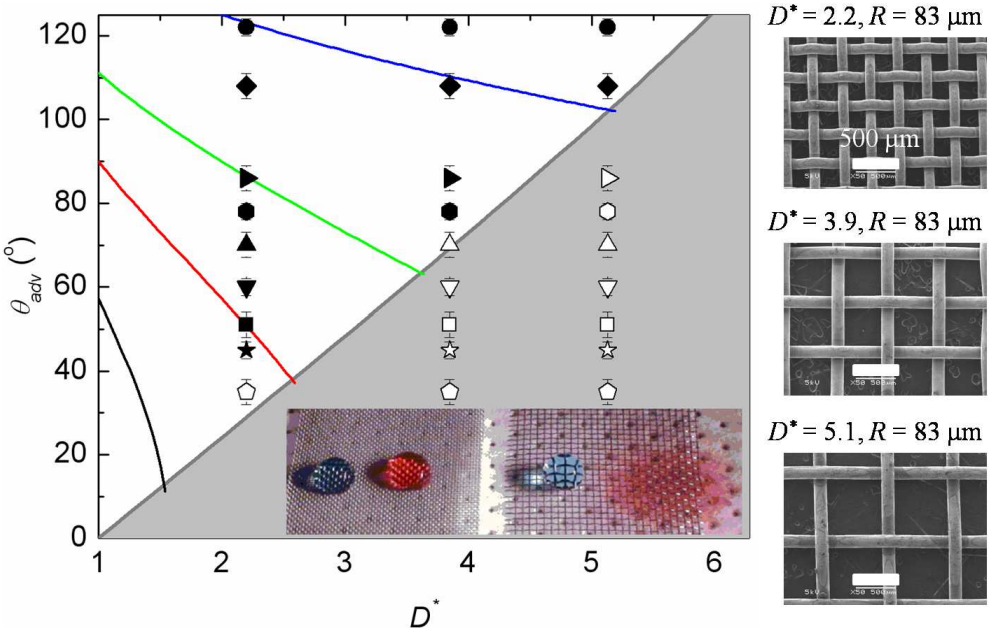

Figure 7. Contact angle data on mesh 70, 40, and 30 (all with R = 83 μm and D^*= 2.2, 3.9, and 5.1 respectively) dip-coated using 50% POSS – 50% Tecnoflon. Contacting liquids include water ((γ_{lv} = 72.1 mN/m), rapeseed oil (γ_{lv} = 35.5 mN/m), hexadecane (γ_{lv} = 27.5 mN/m), dodecane (γ_{lv} = 25.3 mN/m), decane (γ_{lv} = 23.8 mN/m), octane (γ_{lv} = 21.6 mN/m), heptane (γ_{lv} = 20.1 mN/m), and pentane (γ_{lv} = 15.5 mN/m) are plotted on the design chart for liquid wettability. The shaded area represents a set of values for θ_E, D^*, l_{cap}/R which the robustness factor for heptane is less than unity ($A^*_{heptane}$< 1). Filled symbols indicate a liquid droplet with a robust composite interface whereas open symbols indicate a liquid droplet which has transitioned into the fully-wetted interface. The left image in the inset shows nonwetting water (blue, A^*= 14.5) and rapeseed oil (red, A^*= 5.8) droplets with a robust composite interface on a mesh 70 surface (R = 83 μm; D^*= 2.2) coated with 50% POSS – 50% Tecnoflon. The right image shows a water droplet (blue, A^*= 2.1) in a robust composite interface on a mesh 30 (R = 83 μm and D^*= 5.1) surface with a similar coating. Rapeseed oil (red) wets the textured surface because the robustness factor drops to A^*= 0.9. The SEM micrographs of the three textured surfaces are shown on the right.
241x151mm (150 x 150 DPI)

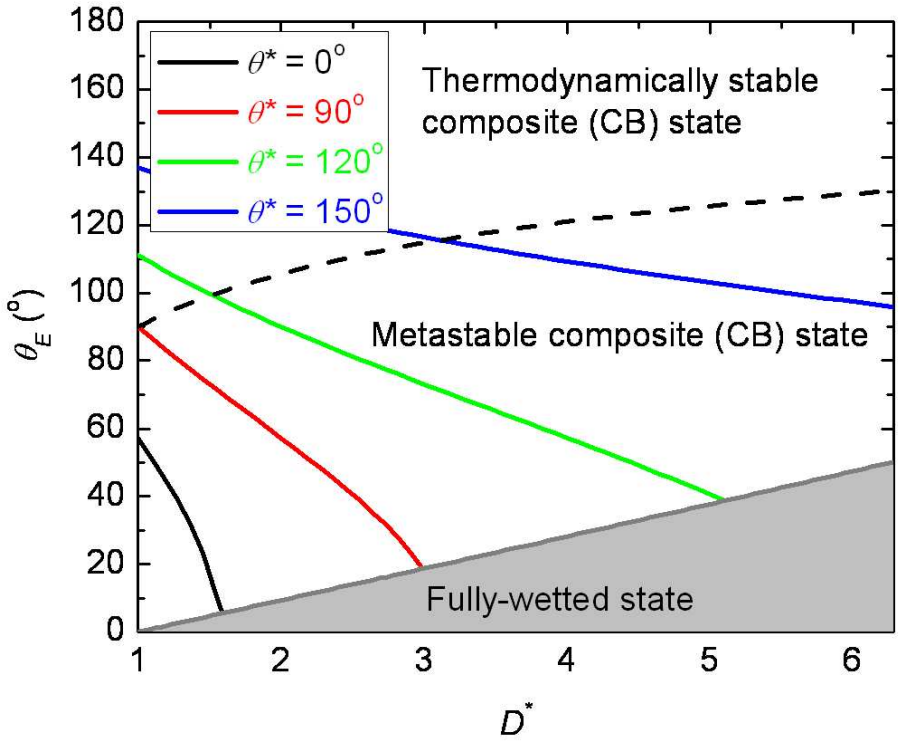

Figure 8. The thermodynamic condition for cross-over from the composite to the fully-wetted interface is shown as the black dashed line on the design chart for liquid wettability. The shaded region indicates parameter space inaccessible for designing non-wetting surfaces with cylindrical textures of length scale R such that $l_{cap}/R = 100$.
187x139mm (150 x 150 DPI)